Received: 4 March 2024 | Revised: 27 June 2024 | Accepted: 28 June 2024

DOI: 10.1002/psc.3645

RESEARCH ARTICLE

Journal of PeptideScience WILEY

Conformational analysis of a new peptide derived from feline immunodeficiency virus gp36 in SDS micelles: An NMR-MD based investigation

Angelo Santoro[1,2] | Michela Buonocore[3] | Mohammad Firoznezhad[4] | Manuela Grimaldi[1] | Anna Maria D'Ursi[1]

[1]Department of Pharmacy, University of Salerno, Fisciano, Italy

[2]Department of Pharmacy, Scuola di Specializzazione in Farmacia Ospedaliera, University of Salerno, Italy

[3]Department of Chemical Sciences and Research Centre on Bioactive Peptides (CIRPeB), University of Naples Federico II, Naples, Italy

[4]Research and Innovation Centre, Fondazione Edmund Mach, San Michele all'Adige, Trento, Italy

Correspondence
Anna Maria D'Ursi, Department of Pharmacy, University of Salerno, via Giovanni Paolo II,132, 84084, Fisciano, Italy.
Email: dursi@unisa.it

Feline immunodeficiency virus (FIV) shares structural similarities with human immunodeficiency virus (HIV): the surface glycoprotein gp36 corresponds to the HIV gp41, which drives virus-host cell interactions and is targeted by the peptide entry inhibitor enfuvirtide. Following a similar drug design strategy for the development of an anti-FIV therapy, the present study investigates $^{627\text{-}646}$gp36 NHR, a peptide sequence derived from a region of gp36 that was previously found to interfere with the antiviral activity of the peptide C8, which instead derives from the gp36 MPER. CD, NMR, and MD simulations were employed to probe the conformational characteristics of $^{627\text{-}646}$gp36 NHR in the membrane-mimicking environment of SDS micelles. Our data show that $^{627\text{-}646}$gp36 NHR is characterized by three dynamic helix structures. MD simulations involving $^{627\text{-}646}$gp36 NHR, C8, and a larger protein, including the CHR and MPER regions, suggest that the interaction of C8 with the MPER region, the origin of the antiviral activity of C8, is disfavored in the presence of $^{627\text{-}646}$gp36 NHR in the simulation. This evidence can be useful for interpreting the molecular mechanism that leads to interference with the activity of C8, providing information on the folding/unfolding mechanism of the viral glycoprotein to design new strategies to inhibit viral entry.

KEYWORDS
feline immunodeficiency virus, FIV, MD simulation, NMR, peptides

1 | INTRODUCTION

Human immunodeficiency virus (HIV) is the etiological agent of acquired immunodeficiency syndrome (AIDS), a disorder characterized by a series of severe infections caused mainly by opportunistic microorganisms and particular neoplastic manifestations (Kaposi's sarcoma, lymphoma).[1–3] Morphologically, HIV is characterized by a 100–120 nm enveloped virus containing a matrix protein and a cone-shaped capsid, with enclosed two single-strand RNA core structures.[4] Among viral glycoproteins surrounding the envelope, encoded by the viral env gene, we found gp160, whose proteolytic cleavage produces gp120, a surface protein with anti-receptor function, and gp41, a transmembrane protein with fusogenic activity, both involved in virus-host cell interaction and viral infection. Despite being a small protein, gp41 presents a peculiar architecture composed of many domains as follows: the fusion peptide (FP), the fusion peptide proximal region

Angelo Santoro and Michela Buonocore contributed equally to this work.

(PR), the N-terminal heptad repeat (NHR), the C-terminal heptad repeat (CHR), a 25–30 residues hydrophobic loop, the membrane-proximal external region (MPER), the transmembrane domain (TM) and the cytoplasmic portion (CP).[5] The virus entry mechanism is based on the rearrangement of NHR and CHR in the trimeric gp41 to assemble a low-energy stable six-helical bundle (6HB)[6–8]; during this process, MPER plays a significant role by correctly driving the virus membrane to blend with the host cell membrane.[9] Among the few medicines approved by the FDA for HIV therapy,[10] we find one of the most known peptide drugs, enfuvirtide (T20, LaRoche®), which derives from the CHR region of gp41 and proved to effectively inhibit the virus entry in the host cell by preventing the correct folding of the viral glycoprotein.[11] HIV is morphologically comparable to other lentiviruses, in particular to the feline immunodeficiency virus (FIV), a lentivirus infecting domestic cats (*Felis catus*)[12] which represents a lethal threat in felines.[13–15] The surface glycoproteins of FIV gp100 (analogous to HIV gp120) and gp36 (analogous to HIV gp41) play critical roles in the early stages of viral entry. Alignment of gp41 and gp36 sequences shows a high degree of homology with a common structural architecture.[16–18] In an attempt to replicate the rational design of enfuvirtide for the development of anti-FIV sequences, several short peptides were previously identified deriving from gp36 sequences, among which C8, an octapeptide deriving from the MPER domain, exhibited significant antiviral activity *in vitro*,[19,20] and whose conformation was studied by nuclear magnetic resonance (NMR) in membrane mimicking micelle solutions.[21] To gain information about the mechanism of action of C8, we obtained the NMR structure of a gp36-deriving construct including the full MPER, the loop, and a small portion of the CHR ($^{737\text{-}786}$gp36 CHR-MPER),[5] which pinpointed the essential role of the three tryptophan residues in the C8 sequence for the interaction with the membrane. Following this approach, we also studied the NHR region, and we focused on an interesting sequence deriving from the residues 627–646 in gp36 (^{627}AGAGTGATAIGMVTQYHQVL^{646}, $^{627\text{-}646}$gp36 NHR), which was previously found to inhibit C8 antiviral activity[20] (Figure 1).

In the hypothesis that this activity may be based on an interaction between $^{627\text{-}646}$gp36 NHR and the region including C8, in this work we report the conformational analysis of the peptide $^{627\text{-}646}$gp36 NHR by circular dichroism (CD) and NMR spectroscopies and molecular dynamics (MD) simulations in a membrane-mimicking system consisting of sodium dodecyl sulfate (SDS) micelle solution. The structure experimentally obtained was then sampled together with the already solved structures of C8[21] and $^{737\text{-}786}$gp36 CHR-MPER (PDB ID: 6FTK)[5] in classical MD simulations in SDS micelles, in order to study the interactions among the three peptides and to gain information about their mechanism of action, whose comprehension is essential in view of the design and optimization of anti-FIV peptide drugs.

2 | MATERIAL AND METHODS

2.1 | Solid-phase peptide synthesis of $^{627\text{-}646}$gp36 NHR

The $^{627\text{-}646}$gp36 NHR peptide was manually synthesized via Fmoc solid-phase synthesis[22] using 200 mg acid resin (Wang) (1.1 mmol/g resin substitution). The resin was swollen in *N*,*N*-dimethylformamide (DMF) for 2 hours at room temperature, then washed with DMF. Next, we added 4 equivalents of hydroxy benzotriazole (HOBT) and hexafluorophosphate benzotriazole tetramethyl uronium (HBTU) and 8 equivalents of *N*,*N*-diisopropylethylamine (DIPEA) as a coupling reagent to the resin to ensure quantitative coupling between the amino acids in the sequence. Deprotection of the Fmoc group was performed by adding 30% piperidine into DMF.[23] To cleave the peptide from the resin and remove all the protecting groups, we used a cleavage cocktail solution containing trifluoroacetic acid (TFA)/H_2O/triisopropylsilane (TIS) (95/2.5/2.5) under stirring for 2 hours. Subsequently, we collected the filtered solution, which was diluted with cold diethyl ether until the precipitation of the product. The product was washed with diethyl ether which was subsequently removed by filtration. The raw product obtained was purified by reverse-phase HPLC, using a Phenomenex C-18 column. The eluent phase consisted of a mixture of H_2O/acetonitrile (ACN) (90/10) with the addition of 0.1% of TFA. A linear gradient of ACN was applied until a final concentration of 90% in 30 min. After collecting the fraction, the purity of the compound was measured by high-resolution mass spectrometry (HR MS) electrospray ionization (ESI).[24]

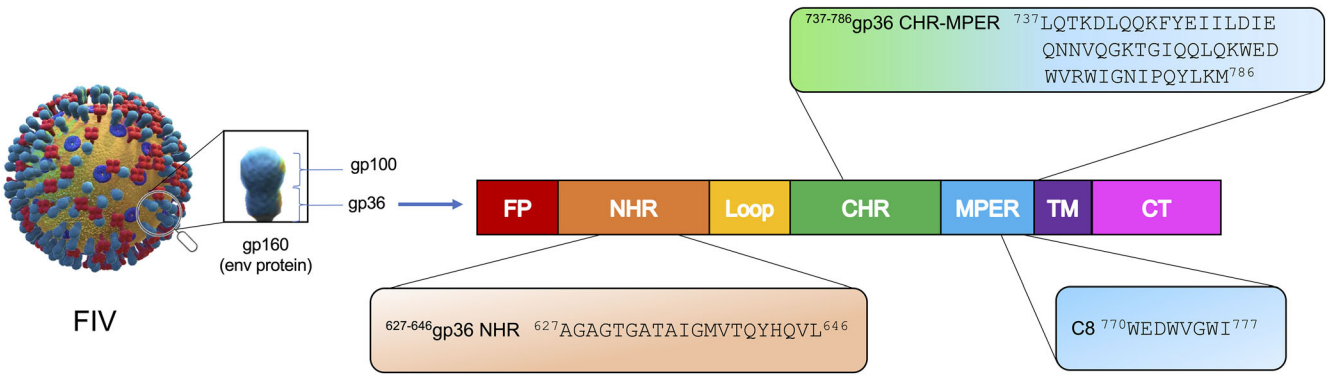

FIGURE 1 Schematic representation of gp36 domains and amino acid sequences of the peptides under investigation.

2.2 | Circular dichroism of $^{627\text{-}646}$gp36 NHR

Circular dichroism (CD) experiments were performed at room temperature on a Jasco-810 spectropolarimeter, working on an average of 4 scans with 10 nm/min scan speed, 4 s response time, 2 nm bandwidth, and 4 accumulations. We used a quartz cuvette with a path length of 1 mm, and a measurement range from 190 to 260 nm (far UV). Throughout the measurements, we ensured a voltage lower than 700 V, which guarantees the reliability of the obtained data. The final concentration of $^{627\text{-}646}$gp36 NHR for CD spectra acquisition was 50 μM in a solution containing SDS micelles (80 mM) in phosphate buffer 20 mM (pH 7.4).

2.3 | Spectra acquisition and assignment of NMR resonances

NMR spectra were recorded on a Bruker Avance II 500 MHz spectrometer. $^{627\text{-}646}$gp36 NHR peptide (3mM) was solubilized in the presence of SDS micelle (80 mM) in phosphate buffer 20 mM at pH 7.4. 2D ^{1}H-^{1}H total ordered correlation spectroscopy (TOCSY) and nuclear Overhauser effect spectroscopy (NOESY) spectra were acquired in the phase-sensitive mode using quadrature detection in ω1 by time-proportional phase incrementation of the initial pulse.[25–27] The ^{1}H-^{13}C heteronuclear single quantum coherence (HSQC) spectrum was also recorded. The water signal was suppressed by excitation sculpting experiments.[28] Experiments were run at 300 K; a mixing time of 80 ms was used for the TOCSY experiments. NOESY experiments were run at 300 K with a mixing time of 200 ms. The assignment of the chemical shifts was obtained using the standard method outlined by Wuthrich, involving the iterative analysis of 2D TOCSY and NOESY spectra, which was performed with the aid of SPARKY software.[29,30] NOESY peaks were integrated using the Gaussian fit integration method of SPARKY software. Hα obtained from NOESY, Cα, and Cβ obtained from HSQC values were uploaded on the CSI 3.0 server (http://csi3.wishartlab.com/)[31] to predict the secondary structure from the chemical shift index (CSI).

2.4 | $^{627\text{-}646}$gp36 NHR structure calculation

The ^{1}H-^{1}H NOESY cross-peaks integrated volumes were converted in XEASY peaks format for the calculation of intramolecular distance restraints and the 3D structure of $^{627\text{-}646}$gp36 NHR with CYANA 3.1.[32] The volumes were converted in upper bound distances using the CALIBA macro. Redundant and duplicate constraints were discarded, and the final list of constraints was used to generate a set of 20 structures using the simulated annealing protocol in torsion angle space (50,000 steps). The best-resulting structures were evaluated according to the lowest target function values (2–20 Å). The structures were visualized using Schrödinger's Maestro 12.5.139.[33]

2.5 | Molecular dynamics

The initial complexes for the molecular dynamics (MD) simulation were obtained with an *ab initio* molecular docking using HADDOCK 2.4 web server.[34] The NMR-derived structures of $^{737\text{-}786}$gp36 CHR-MPER, $^{627\text{-}646}$gp36 NHR and C8 were uploaded as input structures. The four best-ranked complexes were selected according to the HADDOCK score, the number of structures in the cluster, and the RMSD value calculated on the poses compared to the most favorable one in the ensemble. Classical MD simulations were performed with GROMACS[35,36] using CHARMM36 force field.[37] The structures were solvated in explicit TIP4P water. The system in SDS micelles was prepared using the micelle builder in CHARMM-GUI web server,[38] by inserting 200 molecules of SDS and a water thickness of 15 Å. The system was neutralized by adding neutralizing Na^{+} and Cl^{-} ions. After these steps, the energy minimization of the system was performed, and then the system was equilibrated using six cycles of NVT and NpT runs. The system temperature and pressure were kept constant at 300 K and 1.01325 bar using the Berendsen weak coupling method.[39,40] The results were used for MD simulations using Particle Mesh Ewald for long-range electrostatics under NpT conditions.[41] The trajectory files were fitted in the box and converted into PDB coordinates by using the *trjconv* tool of the GROMACS Package. The number of H-bonds and neighbors within 0.35 nm was calculated using the *hbond* tool of GROMACS. Coulomb short-range interaction energies were calculated using the *energy* tool of GROMACS. Solvent-accessible surface area plot was calculated using the *sasa* tool of GROMACS. RMSD values were calculated using the *rms* tool of GROMACS.

3 | RESULTS AND DISCUSSION

3.1 | Structure determination of $^{627\text{-}646}$gp36 NHR peptide

$^{627\text{-}646}$gp36 NHR peptide was obtained using standard solid phase peptide synthesis (SPPS) procedures according to Merrifield's protocol.[42] The peptide conformation was studied in a membrane-mimicking system. Surfactants, such as zwitterionic dodecyl phosphocholine (DPC) or negatively charged SDS, are used to form micelles at concentrations considerably higher than their critical micelle concentration (c.m.c.).[22,43,44] The polar headgroups of these surfactants are found on the surface, and the hydrophobic tails point to the center, forming spherical aggregates. Micelle solutions are widely used as biomimetic membrane systems to study the structural properties of membranotropic molecules. From a technical point of view, they represent ideal systems for CD and NMR analysis in solution, as they tumble sufficiently quickly to result in high-resolution spectral lines. For this conformational analysis, we selected a system composed of pure SDS in a concentration of 80 mM, 10-fold higher than its c.m.c.

3.1.1 | Circular dichroism analysis

To have preliminary information on the conformational properties of $^{627\text{-}646}$gp36 NHR, CD spectra were recorded in SDS micelle solution. Quantitative estimation of CD data was performed on the DichroWeb

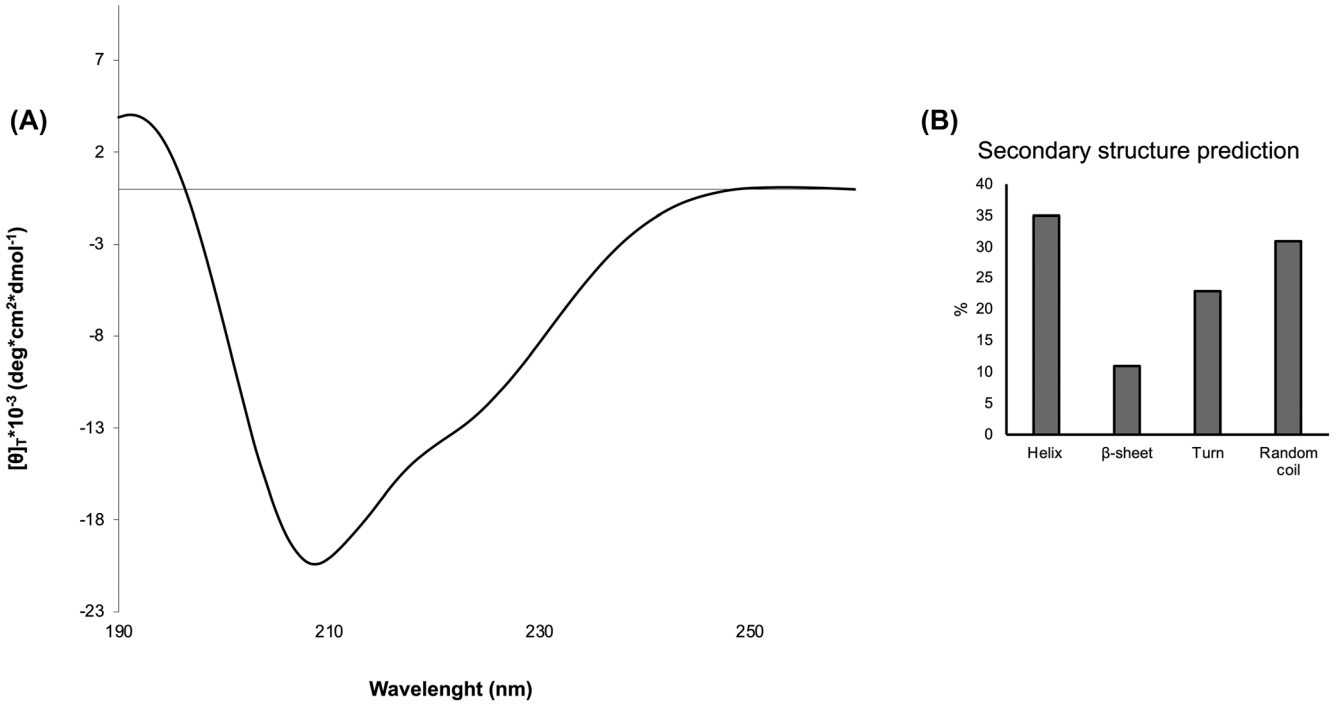

FIGURE 2 (A) CD spectrum of $^{627\text{-}646}$gp36 NHR in SDS acquired using a Jasco J-810 spectropolarimeter at room temperature with a cell path length of 1 mm. The measurement range spans from 190 to 260 nm. (B) Secondary structure prediction of $^{627\text{-}646}$gp36 NHR from the CD curve performed using the CONTIN algorithm.

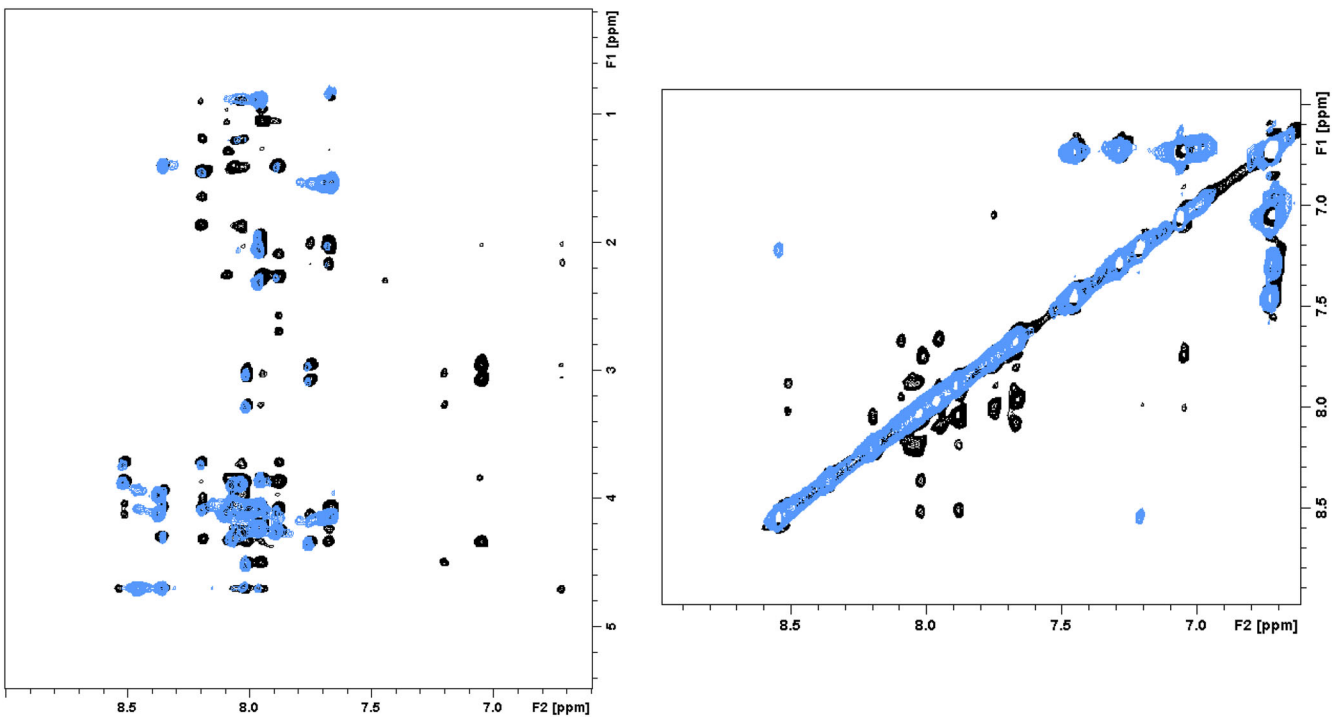

FIGURE 3 Overlap of low field regions in ^{1}H-^{1}H TOCSY (blue) and ^{1}H-^{1}H NOESY (black) of $^{627\text{-}646}$gp36 NHR peptide in SDS micelle solution.

website using the CONTIN algorithm.[45] According to the shape of CD curves and the quantitative evaluation of CD data, $^{627\text{-}646}$gp36 NHR in SDS micelle solution assumes 35% helix, 11% β-sheet, 23% turn, and 31% random coil secondary structure conformation (Figure 2).

3.1.2 | NMR spectroscopy

NMR spectra of $^{627\text{-}646}$gp36 NHR in SDS micelle solution were recorded on a Bruker Avance II 500 MHz spectrometer. Chemical

shift assignments of bidimensional ^{1}H-^{1}H TOCSY and ^{1}H-^{1}H NOESY spectra (Figure 3) were performed according to the procedure of Wüthrich.[25,26,29,30,46]

The values of the proton and carbon chemical shifts derived from NOESY and HSQC are reported in Table S1. The CSI derived from the Δδ of Hα, Cα, and Cβ is reported in Figure S2 and predicts the presence of an α-helix structure between the residues ^{633}A-I^{636}. NOE-derived restraints were extracted from the NOESY spectrum and transformed in interprotonic distances to calculate $^{627\text{-}646}$gp36 NHR 3D structure by simulated annealing calculations using CYANA 3.1 software.[32] Figure 4A summarizes the regular sequential and medium-range NOE effects observed in the NOESY spectrum. NOE patterns on the ^{633}A-H^{643} segment are characterized by the presence of several medium-range NOEs αN(*i*,*i* + 3), αβ(*i*,*i* + 3), and αN (*i*,*i* + 4) that are diagnostics of a helix conformation. This is confirmed by the backbone torsion angle values in the Ramachandran plot (Figure 4B) that are predominantly distributed in the right-handed α-helix region. The best 20 NMR structures selected according to the lowest values of target function were energy minimized, using the distance restraints with a progressively lower force constant.[47] Table 1 summarizes the statistics for the final NMR ensemble. The obtained 3D structure bundle reported in Figure 4C shows that the N-terminus is unordered while the central moiety is

TABLE 1 Statistics for the structural calculation of the NMR ensemble of $^{627\text{-}646}$gp36 NHR peptide.

Number of experimental restraints after CYANA	
Total NOEs	**250**
Intra-residual	178
Sequential	27
Long-range	45
RMSD	
bb/heavy Å	0.73/1.09
Ramachandran analysis	
Favorable regions	74.6%
Additional allowed regions	25.4%
Generously allowed regions	0%
Disallowed regions	0%

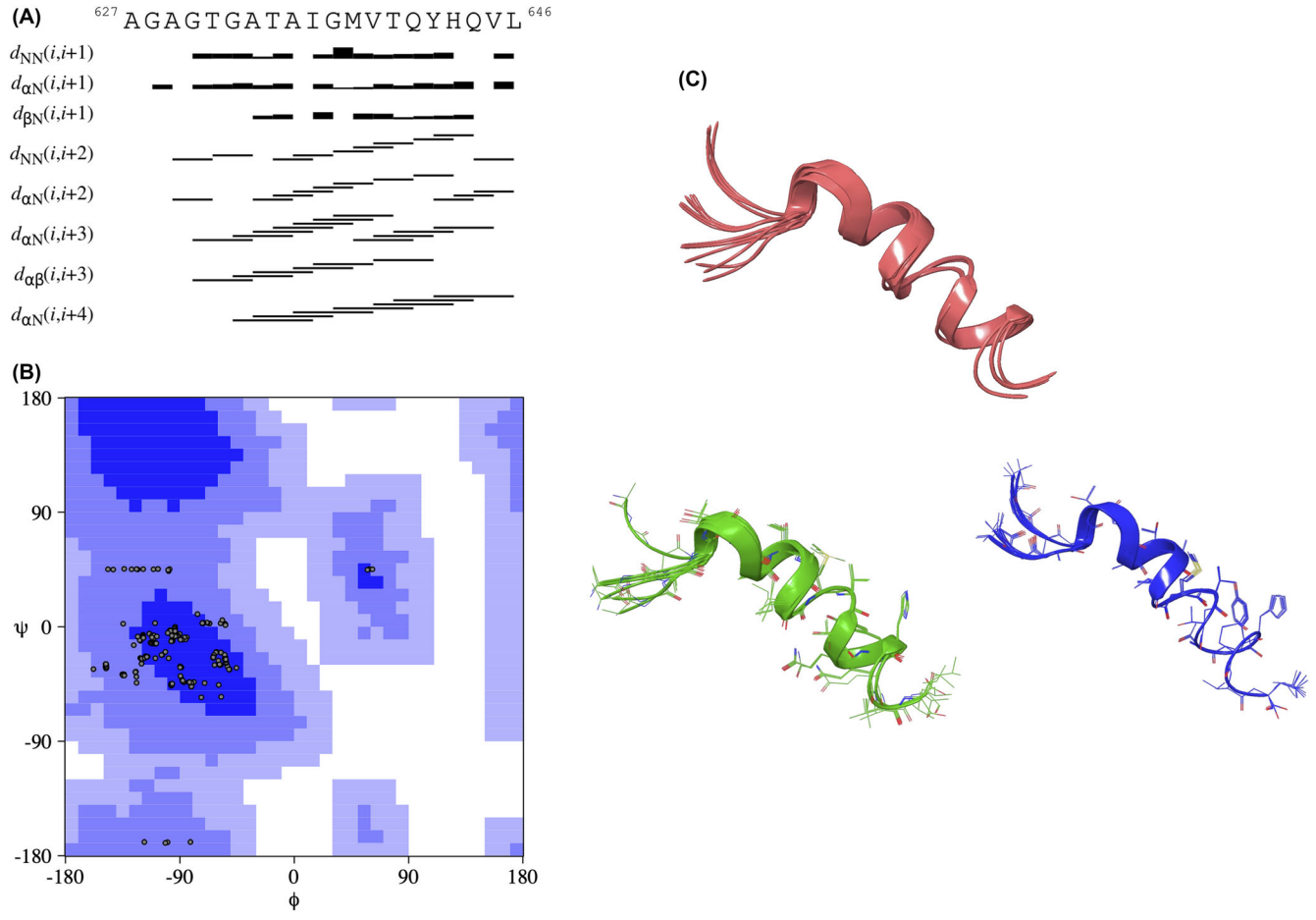

FIGURE 4 (A) Sequential and medium range connectivity collected in NOESY spectra of $^{627\text{-}646}$gp36 NHR in SDS micelle solution. (B) Ramachandran plot of the distribution of ϕ and ψ torsional angles in the ensemble calculated by CYANA. (C) Bundle of the 20 structures (red ribbons) split into two clusters that differ in the presence of an α-helix between the residues ^{640}T-H^{643} (green ribbons) and a 3_{10} helix in the same moiety (blue ribbons).

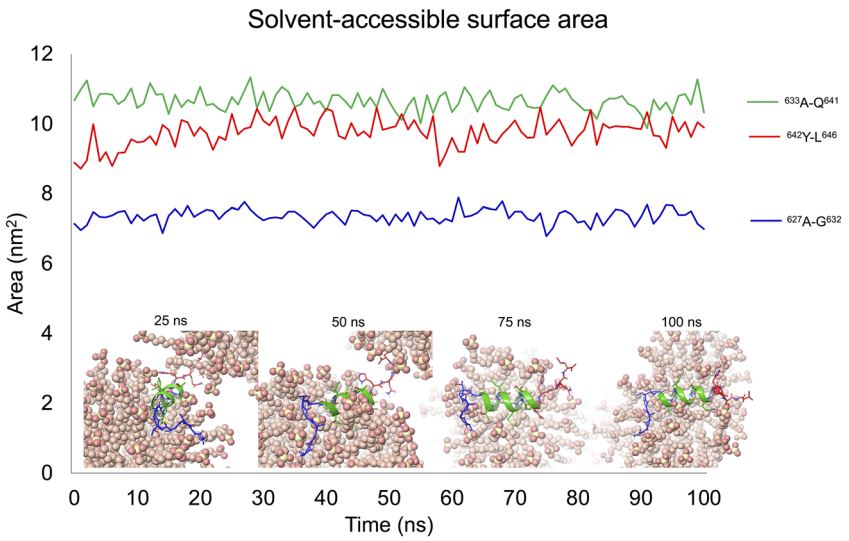

FIGURE 5 Plot reporting the solvent-accessible surface area calculated for the three moieties of $^{627\text{-}646}$gp36 NHR (^{627}A-G^{632} as blue line, ^{633}A-Q^{641} as green line, and ^{642}Y-L^{646} as red line) overlapped with selected snapshots of the trajectory derived from the MD simulation ($^{627\text{-}646}$gp36 NHR moieties are colored as before, SDS micelles are reported in light pink CPK representation, with the sulfur atoms in yellow).

structured in helix conformation with a small turn between the residues ^{629}AG^{630}. The bundle can be further divided into two subclusters, one including a regular α-helix in the residues ^{633}A-H^{643} interrupted by a 3_{10} helix on ^{637}G-V^{639}, and the other including an α-helix in the residues ^{633}A-I^{636} and a 3_{10} helix in the residues ^{637}G-H^{643}.

3.2 | MD simulations

3.2.1 | $^{627\text{-}646}$gp36 NHR in SDS micelles

The NMR solved structure of $^{627\text{-}646}$gp36 NHR was sampled and simulated in classic MD for 100 ns in the presence of polarized water (TIP4P) and micelles composed of 200 SDS molecules in a 450 nm^3 box. The system was prepared using the force field CHARMM36[37] at physiological pH (7.4) and at 300 K. The results consistently describe the structures found in the NMR bundle: for the whole simulation, the peptide holds the α-helix structure in its central moiety, sprawling on the hydrophilic surface of a 45–50 Å diameter micelle, while the N-terminus dynamically interacts with the hydrophobic tails of the micelle, due to its apolar nature, assuming an unstructured conformation with a turn between ^{630}G-G^{632}. The C-terminus instead, which includes two polar uncharged Gln and a polar basic His, in the first steps of the simulation acts as an anchor between the negatively charged surfaces of the multiple SDS micelles that are formed and then ends up being included in the α-helix in the last steps (Figure 5). The plot in the figure quantifies the solvent-accessible surface area of the three moieties under exam: the surface included in N-terminus residues (^{627}A-G^{632}) is less exposed to the water, confirming that it is inserted in the micelles. Differently, the helix moiety (^{633}A-Q^{641}) is rather exposed to the interface micelle/water for the whole simulation, as well as the polar C-terminal tail (^{642}Y-L^{646}), which partly interacts with the negatively charged heads of the SDS molecules and partly is solvated.

3.2.2 | $^{627\text{-}646}$gp36 NHR, $^{737\text{-}786}$gp36 CHR-MPER, and C8 in SDS micelles

The NMR-derived 3D structures of $^{627\text{-}646}$gp36 NHR and C8[21] obtained in SDS micelles and of $^{737\text{-}786}$gp36 CHR-MPER obtained in DPC/SDS 90/10 ratio[5] were docked using HADDOCK2.4 web server.[34,48] The four best-resulting poses from HADDOCK were sampled for 4 250 ns runs (for a total of 1,000 ns) of classical all-atoms MD simulations in SDS micelles. The complexes were prepared for MD as described before. RMSD plot (Figure S3) indicates that the system is equilibrated after 50 ns. From the resulting trajectory reported in Figure 6A, it is possible to see that both C8 and $^{627\text{-}646}$gp36 NHR in the first steps of the concatenate simulation bind $^{737\text{-}786}$gp36 CHR-MPER; in particular, C8 binds non-specifically the target peptide, establishing interactions with the residues on the partial CHR moiety and ending up to prefer the MPER moiety as the simulation proceeds, while $^{627\text{-}646}$gp36 NHR is globally involved in interactions with the region upstream the loop in the largest peptide in the ensemble. However, after around 650 ns, as also indicated by the increase in short-range interaction energies (Figure 6B) and the absence of H-bonds and neighbor contacts for the complex $^{737\text{-}786}$gp36 CHR-MPER/C8 (Figure 6C), the small peptide separates from the largest, while $^{627\text{-}646}$gp36 NHR tends to stabilize its interaction with the partial CHR moiety, with the residues ^{644}Gln, ^{641}Gln and ^{631}Thr involved in transients H-bonds with the amino acids ^{744}Gln, ^{747}Tyr, ^{754}Glu, and ^{753}Gln belonging to $^{737\text{-}786}$gp36 CHR-MPER (Table S2). Remarkably, the interaction between NHR and CHR moieties favors the formation of two ordered α-helices, reproducing the helix bundle that occurs in the full-length protein gp36.

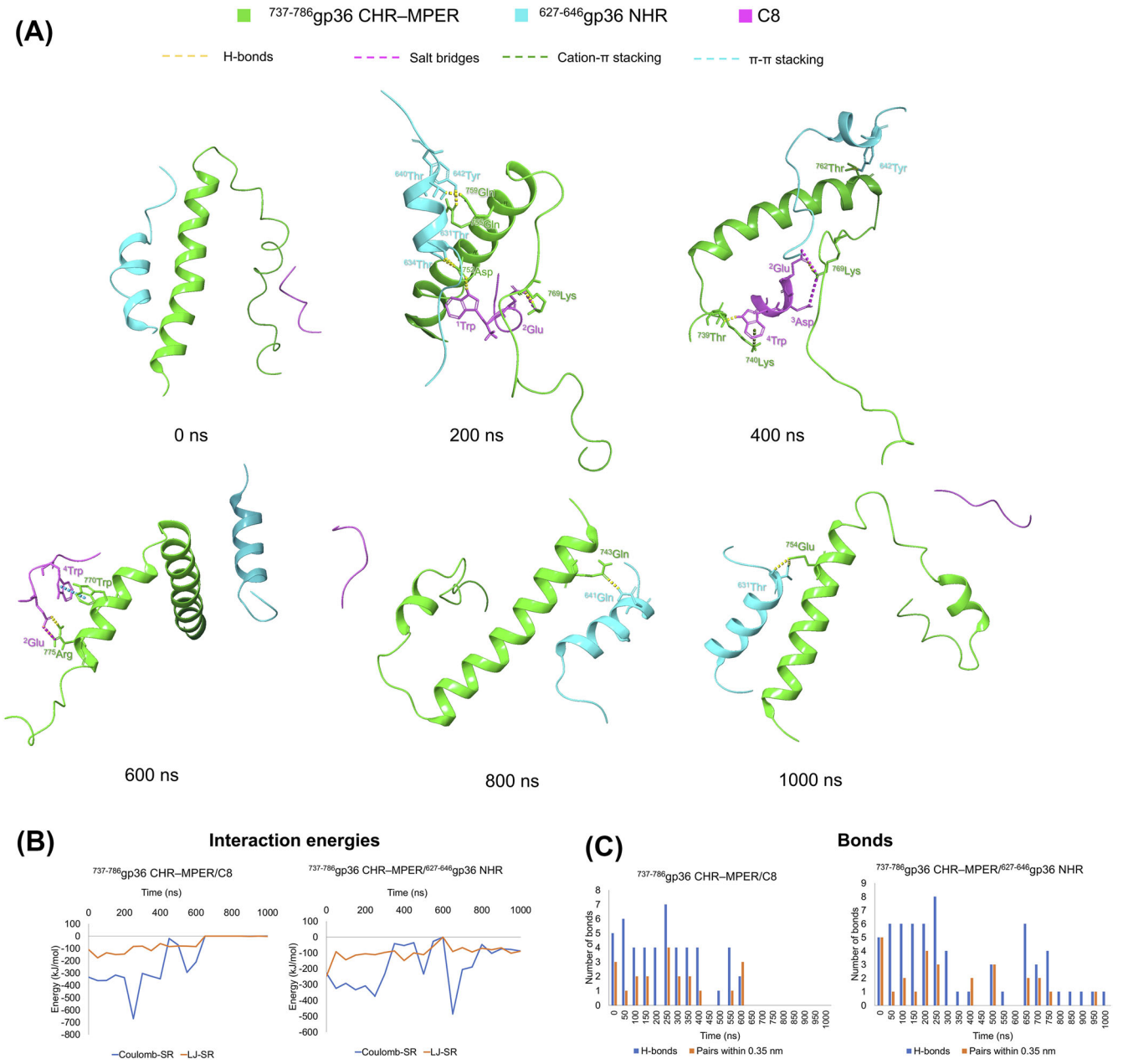

FIGURE 6 (A) Snapshots of selected steps obtained from the concatenate 1,000 ns MD between $^{737\text{-}786}$gp36 CHR-MPER (green ribbon), $^{627\text{-}646}$gp36 NHR (blue ribbon), and C8 (pink ribbon) in SDS micelles. Only the interacting residues are shown in the stick representation. (B) Plotted Coulomb and Lennard-Jones short-range interaction energies for the $^{737\text{-}786}$gp36 CHR-MPER/C8 and $^{737\text{-}786}$gp36 CHR-MPER/$^{627\text{-}646}$gp36 NHR complexes. (C) Graphs reporting the H-bonds and the neighbor pairs (within 0.35 nm) for the $^{737\text{-}786}$gp36 CHR-MPER/C8 and $^{737\text{-}786}$gp36 CHR-MPER/$^{627\text{-}646}$gp36 NHR complexes.

4 | CONCLUSION

Peptides represent a valuable tool in medicinal chemistry, especially in fighting pathogen microorganisms. Among the many FDA-approved peptide drugs targeting viral glycoproteins, we find the enfuvirtide (T20, LaRoche®), a lifesaving therapy against AIDS, which is a 36 amino acids sequence deriving from the HIV's gp41 CHR region and effectively inhibits the viral entry.[49] Hence, following this model, various peptides were designed starting from the sequence of the envelope glycoprotein gp36 of the FIV,[20] a lethal virus with tropism for domestic cats, an animal model suitable for the development of anti-HIV drugs.[50–52] Previously C8, an octapeptide deriving from gp36 MPER with antiviral activity, was identified[19,20] moreover, $^{737\text{-}786}$gp36 CHR-MPER, a larger construct whose NMR-derived 3D structure in DPC/SDS 90/10 M ratio allowed to investigate the involvement of the MPER domain in the folding mechanism.[5] In this

study, we analyze the conformation of $^{627\text{-}646}$gp36 NHR, a 20-residues peptide deriving from the NHR region. Among the previously studied gp36 NHR-deriving sequences, this peptide was the only one demonstrating an effect in interfering with the antiviral activity of C8, reducing its IC_{50} by 25 folds,[20] yet its mechanism of action was never examined. With the aim of enriching the knowledge of the mechanism of the C8 peptide, in this work we focus a structural investigation on $^{627\text{-}646}$gp36 NHR, exploiting its antagonist role to hypothesize its involvement in the binding of C8 with the assumed target $^{737\text{-}786}$gp36 CHR-MPER, using a computational approach starting from experimental coordinates. For this purpose, we started with CD and NMR conformational analysis of $^{627\text{-}646}$gp36 NHR in SDS micelle solution. Our data demonstrate the preference of $^{627\text{-}646}$gp36 NHR to assume helix structure in the central part of the sequence with a short segment of turn between the residues ^{629}AG^{630} and random coil in the N-terminal part. A 100 ns MD simulation in SDS reflects this conformation and, interestingly, points out that the N-terminus is immersed in the core of the micelle, while the central helix lays down on its surface and the C-terminus also interacts with the charged surface of other micelles. The mechanism of linking two or more micelles has been experimentally observed with the peptide C8, which causes the tubulation of multilamellar vesicles (MLVs).[19] This might be a common characteristic among envelope-derived sequences that we will further investigate. Finally, to study the mechanism of action of $^{627\text{-}646}$gp36 NHR in inhibiting the antiviral activity of C8 as experimentally found before, we sampled the NMR-derived structures of $^{627\text{-}646}$gp36 NHR and C8[21] in SDS micelles and of $^{737\text{-}786}$gp36 CHR-MPER in DPC/SDS 90/10 micelles (PDB ID: 6FTK[5]) and performed 1,000 ns classical MD simulation in SDS micelles. The results show that C8 is inclined to non-specifically interact with $^{737\text{-}786}$gp36 CHR-MPER, interacting with residues in both CHR and MPER moieties; however, the binding is undermined by the presence of $^{627\text{-}646}$gp36 NHR, which, in the last steps of the simulation, stabilizes the binding with the partial CHR domain in the target and disfavors the C8 coupling with $^{737\text{-}786}$gp36 CHR-MPER. This behavior is in agreement with the known mechanism of action based on the interaction of the NHR-derived peptide with the CHR moiety.[53,54] The MD results are potentially useful for interpreting the molecular mechanism leading to interference with the C8 peptide's activity, as seen experimentally. In conclusion, the structural analysis of $^{627\text{-}646}$gp36 NHR and its interaction with other domains of gp36 provide insight into the folding/unfolding mechanism of the viral glycoprotein to design new strategies to inhibit viral entry. Moreover, the mechanism of short peptide sequences that have a dual nature and are able to potentially interact with both the inner hydrophobic core and the charged surface of the micelles is an aspect that should be further investigated, as it might be useful in the development of new cell-penetrating sequences, whose advantages in terms of cellular uptake, biocompatibility, versatility, immunogenicity, intracellular targeting, and the potential for combination therapies, make them valuable tools for various biomedical applications.[55] These findings may facilitate the development and optimization of peptide-based drugs targeting FIV, thereby offering potential therapeutic strategies, but also the design of peptide sequences interacting with both the charged surfaces of micelles/vesicles and their hydrophobic cores for different purposes.

CONFLICT OF INTEREST STATEMENT

The authors declare no conflicts of interest.

ACKNOWLEDGEMENTS

Open access publishing facilitated by Universita degli Studi di Salerno, as part of the Wiley - CRUI-CARE agreement.

ORCID

Angelo Santoro https://orcid.org/0000-0002-9690-907X
Michela Buonocore https://orcid.org/0000-0003-1189-1729
Manuela Grimaldi https://orcid.org/0000-0001-7354-8008
Anna Maria D'Ursi https://orcid.org/0000-0001-6814-8472

REFERENCES

1. Ramdial PK, Chetty R, Singh B, Singh R, Aboobaker J. Lymphedematous HIV-associated Kaposi's sarcoma. *J Cutan Pathol*. 2006;33(7):474-481. doi:10.1111/j.1600-0560.2006.00352.x
2. Feller L, Masipa JN, Wood NH, Raubenheimer EJ, Lemmer J. The prognostic significance of facial lymphoedema in HIV-seropositive subjects with Kaposi sarcoma. *AIDS Res Ther*. 2008;5(1):1-6. doi:10.1186/1742-6405-5-2
3. Dauguet M, Lebbé C, Vignes S. Lymphedema and Kaposi sarcoma: a narrative review. *JMV-J Méd Vasc*. 2023;48(5-6):181-187. doi:10.1016/j.jdmv.2023.10.007
4. Dunham SP. Lessons from the cat: development of vaccines against lentiviruses. *Vet Immunol Immunopathol*. 2006;112(1–2):67-77. doi:10.1016/j.vetimm.2006.03.013
5. Grimaldi M, Buonocore M, Scrima M, et al. NMR structure of the FIV gp36 C-terminal heptad repeat and membrane-proximal external region. *Int J Mol Sci*. 2020;21(6):2037. doi:10.3390/ijms21062037
6. Sackett K, Shai Y. The HIV-1 gp41 N-terminal heptad repeat plays an essential role in membrane fusion. *Biochemistry*. 2002;41(14):4678-4685. doi:10.1021/bi0255322
7. Zhang Z, Wang Q, Nguyen HT, et al. Alterations in gp120 glycans or the gp41 fusion peptide-proximal region modulate the stability of the human immunodeficiency virus (HIV-1) envelope glycoprotein pretriggered conformation. *J Virol*. 2023;97(9):e0059223. doi:10.1128/jvi.00592-23
8. Wilen CB, Tilton JC, Doms RW. Molecular mechanisms of HIV entry. *Adv Exp Med Biol*. 2012;726:223-242. doi:10.1007/978-1-4614-0980-9_10
9. Tan K, Liu JH, Wang JH, Shen S, Lu M. Atomic structure of a thermostable subdomain of HIV-1 gp41. *Proc Natl Acad Sci USA*. 1997;94(23):12303-12308. doi:10.1073/pnas.94.23.12303
10. Tompa DR, Immanuel A, Srikanth S, Kadhirvel S. Trends and strategies to combat viral infections: a review on FDA approved antiviral drugs. *Int J Biol Macromol*. 2021;172:524-541. doi:10.1016/j.ijbiomac.2021.01.076
11. Wild CT, Shugars DC, Greenwell TK, McDanal CB, Matthews TJ. Peptides corresponding to a predictive alpha-helical domain of human immunodeficiency virus type 1 gp41 are potent inhibitors of virus infection. *Proc Natl Acad Sci USA*. 1994;91(21):9770-9774. doi:10.1073/pnas.91.21.9770
12. Elder JH, Sundstrom M, de Rozieres S, de Parseval A, Grant CK, Lin YC. Molecular mechanisms of FIV infection. *Vet Immunol Immunopathol*. 2008;123(1–2):3-13. doi:10.1016/j.vetimm.2008.01.007

13. Gomez-Lucia E, Collado VM, Miró G, Martín S, Benítez L, Doménech A. Clinical and hematological follow-up of long-term oral therapy with type-i interferon in cats naturally infected with feline leukemia virus or feline immunodeficiency virus. *Animals*. 2020;10(9):1464. doi:10.3390/ani10091464
14. Stickney A, Ghosh S, Cave NJ, Dunowska M. Lack of protection against feline immunodeficiency virus infection among domestic cats in New Zealand vaccinated with the Fel-O-vax® FIV vaccine. *Vet Microbiol*. 2020;250:108865. doi:10.1016/j.vetmic.2020.108865
15. Rattanabunyong S, Choengpanya K, Suwattanasophon C, et al. Biochemical and structural comparisons of non-nucleoside reverse transcriptase inhibitors against feline and human immunodeficiency viruses. *J Vet Sci*. 2023;24(5):e67. doi:10.4142/jvs.22326
16. Frey SC, Hoover EA, Mullins JI. Feline immunodeficiency virus cell entry. *J Virol*. 2001;75(11):5433-5440. doi:10.1128/JVI.75.11.5433-5440.2001
17. Wyatt R, Sodroski J. The HIV-1 envelope glycoproteins: fusogens, antigens, and immunogens. *Science*. 1998;280(5371):1884-1888. doi:10.1126/science.280.5371.1884
18. Harrison SC. Viral membrane fusion. *Nat Struct Mol Biol*. 2008;15(7):690-698. doi:10.1038/nsmb.1456
19. Grimaldi M, Stillitano I, Amodio G, et al. Structural basis of antiviral activity of peptides from MPER of FIV gp36. *PLoS ONE*. 2018;13(9):e0204042. doi:10.1371/journal.pone.0204042
20. Giannecchini S, di Fenza A, D'Ursi AM, Matteucci D, Rovero P, Bendinelli M. Antiviral activity and conformational features of an octapeptide derived from the membrane-proximal ectodomain of the feline immunodeficiency virus transmembrane glycoprotein. *J Virol*. 2003;77(6):3724-3733. doi:10.1128/JVI.77.6.3724-3733.2003
21. Scrima M, di Marino S, Grimaldi M, et al. Structural features of the C8 antiviral peptide in a membrane-mimicking environment. *Biochim. Biophys. Acta (BBA)-Biomembr*. 2014;1838(3):1010-1018. doi:10.1016/j.bbamem.2013.12.010
22. Mannhold R, Kubinyi H, Folkers G. *BioNMR in drug research*. John Wiley & Sons; 2006.
23. di Micco S, Rahimova R, Sala M, et al. Rational design of the zonulin inhibitor AT1001 derivatives as potential anti SARS-CoV-2. *Eur J Med Chem*. 2022;244:114857. doi:10.1016/j.ejmech.2022.114857
24. Cerqua I, Musella S, Peltner LK, et al. Discovery and optimization of Indoline-based compounds as dual 5-LOX/sEH inhibitors: in vitro and in vivo anti-inflammatory characterization. *J Med Chem*. 2022;65(21):14456-14480. doi:10.1021/acs.jmedchem.2c00817
25. Bax A, Davis DG. MLEV-17-based two-dimensional homonuclear magnetization transfer spectroscopy. *J Magn Reson*. 1985;65(2):355-360. doi:10.1016/0022-2364(85)90018-6
26. Jeener J, Meier BH, Bachmann P, Ernst RR. Investigation of exchange processes by two-dimensional NMR spectroscopy. *J Chem Phys*. 1979;71(11):4546-4553. doi:10.1063/1.438208
27. Piantini U, Sorensen OW, Ernst RR. Multiple quantum filters for elucidating NMR coupling networks. *J Am Chem Soc*. 1982;104(24):6801. doi:10.1021/ja00388a062
28. Parella T, Adell P, Sánchez-Ferrando F, Virgili A. Effective multiple-solvent suppression scheme using the excitation sculpting principle. *Magn Reson Chem*. 1998;36(4):245-249. doi:10.1002/(SICI)1097-458X(199804)36:43.0.CO;2-J
29. Wüthrich K. NMR with proteins and nucleic acids. *Europhys News*. 1986;17(1):11-13. doi:10.1051/epn/19861701011
30. Goddard T, Kneller D. *Sparky 3*. University California; 2004.
31. Hafsa NE, Arndt D, Wishart DS. CSI 3.0: a web server for identifying secondary and super-secondary structure in proteins using NMR chemical shifts. *Nucleic Acids Res*. 2015;43(W1):W370-W377. doi:10.1093/nar/gkv494
32. Güntert P. Automated NMR structure calculation with CYANA. *Protein NMR Techniques*. 2004;353-378. doi:10.1385/1-59259-809-9:353
33. Schrodinger. *Maestro 12.5.139*. Schrodinger LLC; 2018.
34. van Zundert GCP, Rodrigues JPGLM, Trellet M, et al. The HADDOCK2.2 web server: user-friendly integrative modeling of biomolecular complexes. *J Mol Biol*. 2016;428(4):720-725. doi:10.1016/j.jmb.2015.09.014
35. Bekker, H., Berendsen HJ, Dijkstra EJ, Achterop S, Vondrumen RV, Vanderspoel D, Sijbers A, Keegstra H, Renardus MK, Gromacs: a parallel computer for molecular dynamics simulations. 1993.
36. Abraham MJ, Murtola T, Schulz R, et al. GROMACS: high performance molecular simulations through multi-level parallelism from laptops to supercomputers. *SoftwareX*. 2015;1:19-25. doi:10.1016/j.softx.2015.06.001
37. Huang J, MacKerell AD Jr. CHARMM36 all-atom additive protein force field: validation based on comparison to NMR data. *J Comput Chem*. 2013;34(25):2135-2145. doi:10.1002/jcc.23354
38. Jo S, Cheng X, Lee J, et al. CHARMM-GUI 10 years for biomolecular modeling and simulation. *J Comput Chem*. 2017;38(15):1114-1124. doi:10.1002/jcc.24660
39. Berendsen HJ, Postma JP, van Gunsteren WF, Hermans J. Interaction models for water in relation to protein hydration. In: *Intermolecular Forces*. Springer; 1981:331-342. doi:10.1007/978-94-015-7658-1_21
40. Bussi G, Donadio D, Parrinello M. Canonical sampling through velocity rescaling. *J Chem Phys*. 2007;126(1):014101. doi:10.1063/1.2408420
41. Onufriev A, Case DA, Bashford D. Effective born radii in the generalized born approximation: the importance of being perfect. *J Comput Chem*. 2002;23(14):1297-1304. doi:10.1002/jcc.10126
42. Kwon B, Lee M, Waring AJ, Hong M. Oligomeric structure and three-dimensional fold of the HIV gp41 membrane-proximal external region and transmembrane domain in phospholipid bilayers. *J Am Chem Soc*. 2018;140(26):8246-8259. doi:10.1021/jacs.8b04010
43. Pandey S, Alcaro MC, Scrima M, et al. Designed glucopeptides mimetics of myelin protein epitopes as synthetic probes for the detection of autoantibodies, biomarkers of multiple sclerosis. *J Med Chem*. 2012;55(23):10437-10447. doi:10.1021/jm301031r
44. Zerbe O et al. *BioNMR in Drug Research*. Vol. 25. Wiley-VCH Zurich; 2003.
45. Whitmore L, Wallace B. DICHROWEB, an online server for protein secondary structure analyses from circular dichroism spectroscopic data. *Nucleic Acids Res*. 2004;32(suppl_2):W668-W673. doi:10.1093/nar/gkh371
46. Piantini U, Soerensen O, Ernst R. Multiple quantum filters for elucidating NMR coupling networks (Anwendung auf die Anregung von 1, 3-Dibrom-butan). *Chem Inform*. 1983;14(9):6800-6801.
47. Peng JW, Moore J, Abdul-Manan N. NMR experiments for lead generation in drug discovery. *Prog Nucl Magn Reson Spectrosc*. 2004;44(3–4):225-256. doi:10.1016/j.pnmrs.2004.03.001
48. Honorato RV, Koukos PI, Jiménez-García B, et al. Structural biology in the clouds: the WeNMR-EOSC ecosystem. *Front Mol Biosci*. 2021;8:729513. doi:10.3389/fmolb.2021.729513
49. Matthews T, Salgo M, Greenberg M, Chung J, DeMasi R, Bolognesi D. Enfuvirtide: the first therapy to inhibit the entry of HIV-1 into host CD4 lymphocytes. *Nat Rev Drug Discov*. 2004;3(3):215-225. doi:10.1038/nrd1331
50. Burkhard MJ, Dean GA. Transmission and immunopathogenesis of FIV in cats as a model for HIV. *Curr HIV Res*. 2003;1(1):15-29. doi:10.2174/1570162033352101
51. Miller C, Abdo Z, Ericsson A, Elder J, VandeWoude S. Applications of the FIV model to study HIV pathogenesis. *Viruses*. 2018;10(4):206. doi:10.3390/v10040206

52. Yamamoto JK, Sanou MP, Abbott JR, Coleman JK. Feline immunodeficiency virus model for designing HIV/AIDS vaccines. *Curr HIV Res*. 2010;8(1):14-25. doi:10.2174/157016210790416361
53. Aisenbrey C, Bechinger B. Structure, interactions and membrane topology of HIV gp41 ectodomain sequences. *Biochim Biophys Acta Biomembr*. 2020;1862(7):183274. doi:10.1016/j.bbamem.2020.183274
54. Lakomek NA, Kaufman JD, Stahl SJ, et al. Internal dynamics of the homotrimeric HIV-1 viral coat protein gp41 on multiple time scales. *Angew Chem Int Ed Engl*. 2013;52(14):3911-3915. doi:10.1002/anie.201207266
55. Desale K, Kuche K, Jain S. Cell-penetrating peptides (CPPs): an overview of applications for improving the potential of nanotherapeutics. *Biomater Sci*. 2021;9(4):1153-1188. doi:10.1039/D0BM01755H

SUPPORTING INFORMATION

Additional supporting information can be found online in the Supporting Information section at the end of this article.

How to cite this article: Santoro A, Buonocore M, Firoznezhad M, Grimaldi M, D'Ursi AM. Conformational analysis of a new peptide derived from feline immunodeficiency virus gp36 in SDS micelles: An NMR-MD based investigation. *J Pept Sci*. 2024;30(12):e3645. doi:10.1002/psc.3645